NUMERICAL STUDY OF TWO-PHASE FLOWS IN MICROCHANNELS USING THE LEVEL SET METHOD

Mahidhar Tatineni* **and Xiaolin Zhong†**
University of California, Los Angeles, California 90095

ABSTRACT

There is considerable ongoing research on multiphase flows in microfluidic systems. This paper presents a numerical procedure for studying two phase flows in microchannels based on the level set method. Incompressible Navier-Stokes equations are used in both the gas and liquid phases. The interface is computed as the zero level set and the level set function is computed using a level set advection equation. The numerical scheme is based on a standard staggered MAC grid for discretization. The spatial discretization is carried out by using a fifth order WENO scheme for the convective terms and a second order discretization for all other terms. The numerical procedure was validated using comparisons with existing numerical studies and with a grid independence study. The numerical simulations are used to study a cross-shaped gas/liquid mixing section which produces monodisperse gas bubbles coflowing with liquids in a micro-channel. The surface tension, liquid flow rates and gas flow rates are varied and their effects on the bubble sizes and frequencies are studied. The numerical results are compared and found to be in good agreement with existing experimental results.

1 INTRODUCTION

Currently, there is considerable ongoing research on multiphase flows in microfluidic devices. This paper uses numerical simulations as a tool for studying two phase flows in microchannels. In part, this research is being applied in studying two phase flows in micro direct methanol fuel cells. There are significant two-phase flow effects on both the anode and cathode side. In the anode channel the liquid methanol fuel exists with the carbondioxide bubbles generated by the chemical reaction as follows:

$$CH_3OH + H_2O \rightarrow CO_2 + 6H^+ + 6e^- \quad (1)$$

On the cathode side the air drawn in from the ambient exists with the water droplets formed due to the chemical reaction as follows:

$$6H^+ + 6e^- + 3/2O_2 \rightarrow 3H_20 \quad (2)$$

Hence, an effective design of the methanol micro fuel cells needs a good understanding of such two-phase flows in micro channels. In addition, the carbon-dioxide gas produced in the micro fuel cell is breathed out using a gas-liquid separator. In order to understand such two-phase flows an experiment was designed by Cubaud et. al. [1] which uses an innovative gas/liquid mixing section to produce gas bubbles coflowing with liquid in microchannels. Previous experimental studies used absolute instabilities in gas microligaments coflowing in a focused liquid stream to produce micro bubbles via a self excited breakup phenomenon[2, 3]. In this paper, we present a numerical procedure to study two-phase flows in microfluidic devices and use it to study flows in the above mentioned mixing section and the production of gas bubbles due to the liquid crossflow.

Level set based numerical methods are becoming attractive for simulations of multiphase or multimaterial incompressible flows with complex topological changes [4, 5, 6, 7, 8]. For micro scale flows one of the issues is the high resolution requirements for the interface. The adaptive level set method [9] was developed for achieving higher resolution in the required regions with minimum additional cost. Further improvement was made by Sussman and Puckett [10] who developed a coupled level set and volume of fluid method and used it to compute flows in microscale jetting devices. This approach was later extended to a second order coupled level set and volume of fluid method by Sussman [11]. The first level set methods for two-phase flows [4, 5] were based on using a continuous surface tension model for the two-phase flows. That is, the discontinuity in pressure across

*Staff Research Associate, Mechanical and Aerospace Engineering Department, Member AIAA.
†Professor, Mechanical and Aerospace Engineering Department, Associate Fellow AIAA, xiaolin@seas.ucla.edu.

a multiphase interface is smeared into a numerically continuous function. This approach may give rise to non-physical parasitic flows which can lead to errors in the overall flow velocities [7]. In [6], the Ghost Fluid Method (GFM) was developed to capture the jump conditions across a contact discontinuity without such numerical smearing. This idea was extended to multiphase incompressible flows by Kang et. al. [7]. They presented a numerical scheme which takes into account the jumps in the flow properties and the pressure discontinuities across multiphase interfaces. The pressure Poisson equation was modified to include the pressure jump conditions to effectively solve this problem. In this paper we consider both the continuous model and the boundary condition capturing methods to solve the pressure poisson equation.

In this paper we use level set method based simulations to study two-phase flows in micro channels. The governing equations are based on the incompressible Navier-Stokes equations in both fluids with jump conditions at the multiphase interface. In addition, the level set equation is also solved to keep track of the interface. The equations are discretized on a standard MAC grid with velocities on cell walls and the rest of the properties at the cell centers. A fifth order WENO discretization [6] is used for the convective terms and a second order discretization is used for the viscous terms. The pressure poisson equation is solved using a multigrid iterative solver. The numerical simulations are used to study gas/liquid flow in square microchannels and the results compared with experimental results.

2 GOVERNING EQUATIONS

2.1 Incompressible N-S Equations for the Two Phases

The basic equations used in the simulations are the incompressible Navier-Stokes equations with the gravitational term and jump conditions at the multimaterial interface. The viscous incompressible equations are:

$$\frac{\partial \rho}{\partial t} + \vec{V}.\nabla \rho = 0 \tag{3}$$

$$\frac{\partial u}{\partial t} + \vec{V}.\nabla u + \frac{p_x}{\rho} = \frac{(2\mu u_x)_x + (\mu(u_x + v_y))_y + (\mu(u_z + w_x))_z}{\rho} \tag{4}$$

$$\frac{\partial v}{\partial t} + \vec{V}.\nabla v + \frac{p_y}{\rho} = \frac{(\mu(u_y + v_x))_x + (2\mu v_y)_y + (\mu(v_z + w_y))_z}{\rho} + g \tag{5}$$

$$\frac{\partial w}{\partial t} + \vec{V}.\nabla w + \frac{p_z}{\rho} = \frac{(\mu(w_x + u_z))_x + (\mu(v_z + w_y))_y + (2\mu w_z)_z}{\rho} \tag{6}$$

where t is the time, (x,y,z) are the spatial coordinates, ρ is the density, $\vec{V} =< u, v, w >$ is the velocity field, p is the pressure, μ is the viscosity, and g is the gravity. The viscosity and density parameters are different in the two fluids. The velocity is continuous across the multiphase interface. However, when calculating the viscous terms and solving the pressure poisson solver the jump conditions across the interface need to be calculated. The equations for the jump conditions were derived by Kang et. al. [7] as follows:

$$\left[\frac{p_x}{\rho}\right] = \left[\frac{(2\mu u_x)_x + (\mu(u_x + v_y))_y + (\mu(u_z + w_x))_z}{\rho}\right] \tag{7}$$

$$\left[\frac{p_y}{\rho}\right] = \left[\frac{(\mu(u_y + v_x))_x + (2\mu v_y)_y + (\mu(v_z + w_y))_z}{\rho}\right] \tag{8}$$

$$\left[\frac{p_z}{\rho}\right] = \left[\frac{(\mu(w_x + u_z))_x + (\mu(v_z + w_y))_y + (2\mu w_z)_z}{\rho}\right] \tag{9}$$

$$[p] - [\mu](\nabla u.\vec{N}, \nabla v.\vec{N}, \nabla w.\vec{N}).\vec{N} = \sigma\kappa \tag{10}$$

where σ is the surface tension, and κ is the curvature of the interface. The interface is tracked using the level set equation:

$$\frac{\partial \phi}{\partial t} + \vec{V}.\nabla \phi = 0 \tag{11}$$

where $\phi = 0$ represents the interface location. To keep the values of ϕ close to that of a signed distance function the level set function is reinitialized after every time step using iterations in a pseudo time variable:

$$\frac{\partial \phi}{\partial \tau} + S(\phi_o)(|\nabla \phi| - 1) = 0 \tag{12}$$

The level set function is used to compute the normal vector and the interface curvature as follows:

$$\vec{N} = \frac{\nabla \phi}{|\nabla \phi|} \tag{13}$$

$$\kappa = -\nabla.\vec{N} \tag{14}$$

2.2 Continuous Form

In this paper we mainly use the continuous form of the equations without the jump conditions[4, 12]. In the continuous case the viscosity and density are expressed as functions of the level set function as follows:

$$\mu(\phi) = \mu^- + (\mu^+ - \mu^-)H(\phi) \quad (15)$$

$$\rho(\phi) = \rho^- + (\rho^+ - \rho^-) \quad (16)$$

where $H(\phi)$ is a Heaviside function based on ϕ defined as follows:

$$H(\phi) = \begin{cases} 0 & \phi < -\epsilon \\ \frac{1}{2} + \frac{\phi}{2\epsilon} + \frac{1}{2\pi}\sin(\frac{\pi\phi}{\epsilon}) & -\epsilon \le \phi \le \epsilon \\ 1 & \phi > \epsilon \end{cases} \quad (17)$$

and μ^-, ρ^- represent the fluid where $\phi \le 0$ and μ^+, ρ^+ represent the fluid where $\phi > 0$. Using the continuous surface force model the pressure is continuous and the remaining jump conditions can be modeled by adding a term of the form

$$\frac{\delta\sigma\kappa\vec{N}}{\rho} \quad (18)$$

to the right hand side of the momentum equations. Note that now the delta function is also smeared out and calculated by taking a derivative of the above Heaviside function.

3 NUMERICAL METHOD

The discretization of the above equations is performed using a standard MAC grid. The velocities exist at the appropriate cell walls and the pressure, density, viscosity and level set function are defined at the cell center. The incompressible solver is based on a projection method and the time advancement is carried out using a 3rd order TVD Runge-Kutta method. The convective terms are discretized using a 5th order WENO scheme following the approach of Fedkiw et. al. [6]. For the viscous terms both the continuous delta function approach and the jump conditions approach is used based on the work of Kang et. al. [7]. In the projection method the pressure is solved using the variable coefficient Poisson equations developed in [6]. The resulting poisson equation is solved using a multigrid Gauss-Seidel iterative method.

The numerical procedure has been modified to consider slipping and dynamic contact lines using models. However, in this paper all the simulations assume no contact of the 2-phase boundary with the walls of the microchannels. This is a reasonable assumption for the current study since the experimental cases we compared the results with showed no dewetting and the bubbles were lubricated by a thin liquid film and there were no contact lines.

4 RESULTS

The numerical code based on the level set method has been developed and tested. The code was first validated by considering the test case of a rising air bubble in water used by Kang et. al. [7] with various grid sizes. The validated code was then used to compute the 2-phase flows in the gas/liquid mixing section studied experimentally by Cubaud et. al.[1]. In the experiment there is gas flowing through a microchannel. The liquid is introduced from two sides of the microchannel (forming a cross like section) to pinch the gas flow and form bubbles. In the experiment the gas and liquid flow rates are changed and their effects on the bubbles are studied by high speed camera photos. The numerical results are compared with the experimental results for the bubble sizes and frequencies and found to be in good agreement.

4.1 Validation Cases

Rise of Air Bubble in Water

For the validation case the rise of a circular air bubble of radius 1/300m in water was considered. The computational domain was of size [-0.01m,0.01m] x [-0.01m,0.02m] and initially the bubble is located at the origin. The computation was carried out with mesh sizes of 40×60, 80×120, 100×100, 160×240, 200×200, and 300×300. Figure 1 shows a sequence of plots in time detailing the rise of the air bubble. The deformation and movement of the air-water interface can be clearly seen as the bubble rises in water. Figure 2 shows the velocity contours for the flowfield at $t = 0.05s$ obtained using the smeared delta function method. This case was computed by Kang et.al. [7] and Fig. 3 shows the comparison with our results of the bubble interface at $t = 0.05s$. The interface location and the rise of bubble are found to be in good agreement. The accuracy of the scheme can be measured quantitatively for the various mesh sizes by checking the area loss for each case. The results are tabulated in Table 1. From the results it is clear that the area loss is reducing to smaller values as the grid is made finer. The error in the area drops from 16.68% to 0.22% as the grid size is increased from 40×60 to 300×300.

Grid Independence Study for 2-D Simulations

The validated level set code was used for the simulations of two phase flows in a micro gas/liquid crossflow

section. To evaluate the grid independence of the computations a 2-D test case with a gas velocity of $0.1m/s$ and a liquid crossflow velocity of $0.5m/s$ in a $100\mu m$ by $500\mu m$ channel was computed with grid sizes of 33×161, 65×321, 129×641. Figure 4 shows the development of the gas bubble and the subsequent pinching off due to the crossflow for the three grid sizes. Clearly, the two finer grids are in very good agreement with regards to the bubble size and development rate. The quantitative comparisons for the bubble size and frequency are presented in Table 2. The coarsest grid leads to a difference of 7.08% in bubble size with respect to the finest grid. However, the frequency of the bubble shedding agrees within 1% even with the coarse grid. With the double grid (65×321) case the errors in both frequency and bubble size are less than 0.1%. Hence, the numerical simulations show good convergence with increasing grid sizes. The two dimensional grid independence study is used to determine the appropriate number of grid points for an accurate computation of the flows in the 3-D gas/liquid mixing section.

4.2 Simulations of Flows in Gas/Liquid Mixing Section

The level set code, validated with comparisons with existing results and grid independence studies, is used to investigate the formation of the air bubbles by the break up of a air stream in a microchannel by a crossflow of water from two sides of the microchannel. First, 2-D simulations were carried out to investigate the ability of the code to predict the growth of the gas interface and the pinching process to produce micro bubbles. In addition, the surface tension coefficient was varied to investigate its effect on the size of the bubbles produced. Finally, full 3-D simulations are conducted for various gas and liquid flow rates and the results are compared with the experimental results of Cubaud et. al.[1].

2-D Simulation Results

The 2-D simulations were used in the grid independence study detailed above. In addition, we also used the 2-D simulations to study the effect of varying the surface tension on the bubble sizes and frequencies. The test cases considered air flow in a channel with water crossflow. The surface tension was changed as $\sigma = 0.0728kg/s^2, \sigma = 0.01456kg/s^2$, and $\sigma = 0.1456kg/s^2$. The densities and viscosities were kept the same as the air and water values. Figure 5 shows a sequence of plots of the air-water interface, with the pressure contours, to show the pinching process and the formation of the bubble. Figure 6 shows the pinching process for the lower surface tension case. The bubble formed in this case is much smaller than the previous case. When the surface tension is increased, the bubble formed is longer as shown in Fig. 7. Hence, the surface tension is one of the controlling factors in the size of the bubble formed. The results from the 2-D simulations are also tabulated in Table 3 which shows the length of the bubbles formed in each case.

3-D Simulation Results

The 3-D simulations were conducted for various gas and liquid flow rates to evaluate the bubble sizes and frequencies. From the experimental results one of the important controlling parameter was found to be the homogeneous liquid fraction $\alpha_L = \frac{Q_L}{Q_L+Q_G}$. The numerical simulations were conducted for homogeneous liquid fractions of 0.5, 0.67, and 0.8. The results were then compared with the experimental results. Figure 8 shows a sequence of plots corresponding to various instants in time, for the $\alpha_L = 0.5$ case. The gas-liquid interface is plotted in the figures. The elongation of the interface and the subsequent pinching due to the liquid crossflow can be clearly seen. The size of the bubble pinched off is about 1.9 times the channel width. Figure 9 shows pinching process for a higher homogeneous liquid fraction of 0.67. The bubble size is now reduced since the faster liquid velocity results in a quicker pinching of the bubble. When the α_L value is further increased to 0.8 the bubble size is also further reduced. In addition, there is significant deformation of the bubble once it is pinched due to the high liquid velocities pushing it.

Hence, based on the above results, we can conclude that the bubble size can be effectively controlled by varying the homogeneous liquid fraction. As seen from the simulation results, currently the computational domain is too small to compute the pinching of multiple bubbles and the distance between the bubbles for various flow rates. We are currently conducting simulations with longer domains to be able to simulate longer bubbles (of the order of 10 times the channel width) and to simulate multiple bubbles being pinched off in succession.

From the numerical simulations we have obtained the bubble sizes for various liquid fraction values and compared them with existing experimental results [1] as shown in Fig. 11. The results show that the numerical simulations are in good agreement with experimental results and the correlation developed based on experimental results. The numerical results are found to be within the experimental scatter. It should be noted that the numerical results for the 3-D cases were computed with the coarse grid (as compared with the 2-D grid in-

dependence study) of $33 \times 161 \times 33$. Computations are in progress with finer grids and the comparisons with the experimental results are expected to further improve.

Hence, the 3-D simulations were able to capture the gas/liquid interface development and pinching process observed in the experimental studies. The bubble sizes obtained from the numerical studies are in good agreement with the corresponding experimental results.

5 CONCLUSIONS

A numerical procedure has been developed based on the level set method for simulating two-phase flows in microchannels. The method has been validated by computing test cases with various grid sizes and checking for grid independence. Results of both 2-D and 3-D simulations of two-phase flow computations in micro channels have been presented. The results show that the gas and liquid flow rates can be adjusted to produce gas bubbles of varying sizes coflowing with liquid in microchannels. The numerical simulation results for bubble sizes were found to be in good agreement with existing experimental results. Further studies are in progress to understand the bubble pinching and transport processes in microchannels.

6 ACKNOWLEDGMENTS

The authors are grateful to Dr. Thomas Cubaud of UCLA for his assistance and for providing the results of his experimental studies. The research presented in the paper is supported by DARPA under the DARPA Micro Power Generation (MPG) program with Dr. Clark T.-C. Nguyen as the program manager.

References

[1] Cubaud, T. and Ho, C.-M., "Transport of bubbles in square microchannels," *presented at the Divison of Fluid Dynamics 56th Annual Meeting, East Rutherford, New Jersey, Nov 23-25*, 2003.

[2] Ganan-Calvo, A. M. and Gordillo, J. M., "Perfectly Monodisperse Microbubbling by Capillary Flow Focusing," *Physical Review Letters*, Vol. 87(27), 2001.

[3] Gordillo, J. M. and Ganan-Calvo, A. M., "Monodisperse microbubbling: Absolute instabilities in coflowing gas-liquid jets," *Physics of Fluids*, Vol. 13(12), 2001, pp. 3839–3842.

[4] Sussman, M., Smereka, P., and Osher, S., "A Level Set Approach for Computing Solutions to Incompressible Two-Phase Flow," *Journal of Computational Physics*, Vol. 114, 1994, pp. 146–154.

[5] Chang, Y. C., Hou, T. Y., Merriman, B., and Osher, S., "A Level Set Formulation of Eulerian Interface Capturing Methods for Incompressible Fluid Flows," *Journal of Computational Physics*, Vol. 124, 1996, pp. 449–464.

[6] Fedkiw, R., Aslam, T., Merriman, B., and Osher, S., "A Non-Oscillatory Eulerian Approach to Interfaces in Multimaterial Flows (The Ghost Fluid Method)," *Journal of Computational Physics*, Vol. 152, 1999, pp. 457–492.

[7] Kang, M., Fedkiw, R. P., and Liu, X.-D., "A Boundary Condition Capturing Method for Multiphase Incompressible Flow," *Journal of Scientific Computing*, Vol. 15, 2000, pp. 323–360.

[8] Aalburg, C., "Deformation and Breakup of Round Drops and Nonturbulent Liquid Jets in Uniform Crossflows," *Ph.D. Thesis, Aerospace Engineering and Scientific Computing, University of Michigan*, 2002.

[9] Sussman, M., Almgren, A. S., Bell, J. B., Colella, P., Howell, L. H., and Welcome, M. L., "An Adaptive Level Set Approach for Incompressible Two-Phase Flows," *Journal of Computational Physics*, Vol. 148, 1999, pp. 81–124.

[10] Sussman, M. and Puckett, E. G., "A Coupled Level Set and Volume-of-Fluid Method for Computing 3D and Axisymmetric Incompressible Two-Phase Flows," *Journal of Computational Physics*, Vol. 162, 2000, pp. 301–337.

[11] Sussman, M., "A second order coupled level set and volume-of-fluid method for computing growth and collapse of vapor bubbles," *Journal of Computational Physics*, Vol. 187, 2003, pp. 110–136.

[12] Brackbill, J. U., Kothe, D. B., and Zemach, C., "A Continuum Method for Modeling Surface Tension," *Journal of Computational Physics*, Vol. 100, 1992, pp. 335–354.

Table 1: **Area loss variation with grid size for computations of rise of air bubbles in water**

Grid Size	Area Loss
40×60	16.68%
100×100	7.12%
80×120	5.39%
200×200	1.92%
160×240	1.55%
300×300	0.22%

Table 2: **Variation of bubble sizes and frequencies with grid sizes. Gas velocity set at 0.1 m/s, and liquid velocity fixed at 0.5 m/s. The comparisons are made with the finest grid as reference.**

Grid Size	Bubble Size	Frequency
33×161	7.08%	1%
65×321	$< 0.1\%$	$< 0.1\%$
129×641	-	-

Table 3: **Variation of bubble sizes with surface tension. Gas velocity set at 0.1 m/s, and liquid velocity fixed at 0.5 m/s.**

Surface Tension (Kg/s^2)	(Bubble Length)/(Channel Width)
0.0728	1.219
0.0728/5	0.685
$0.0728 * 2$	1.419

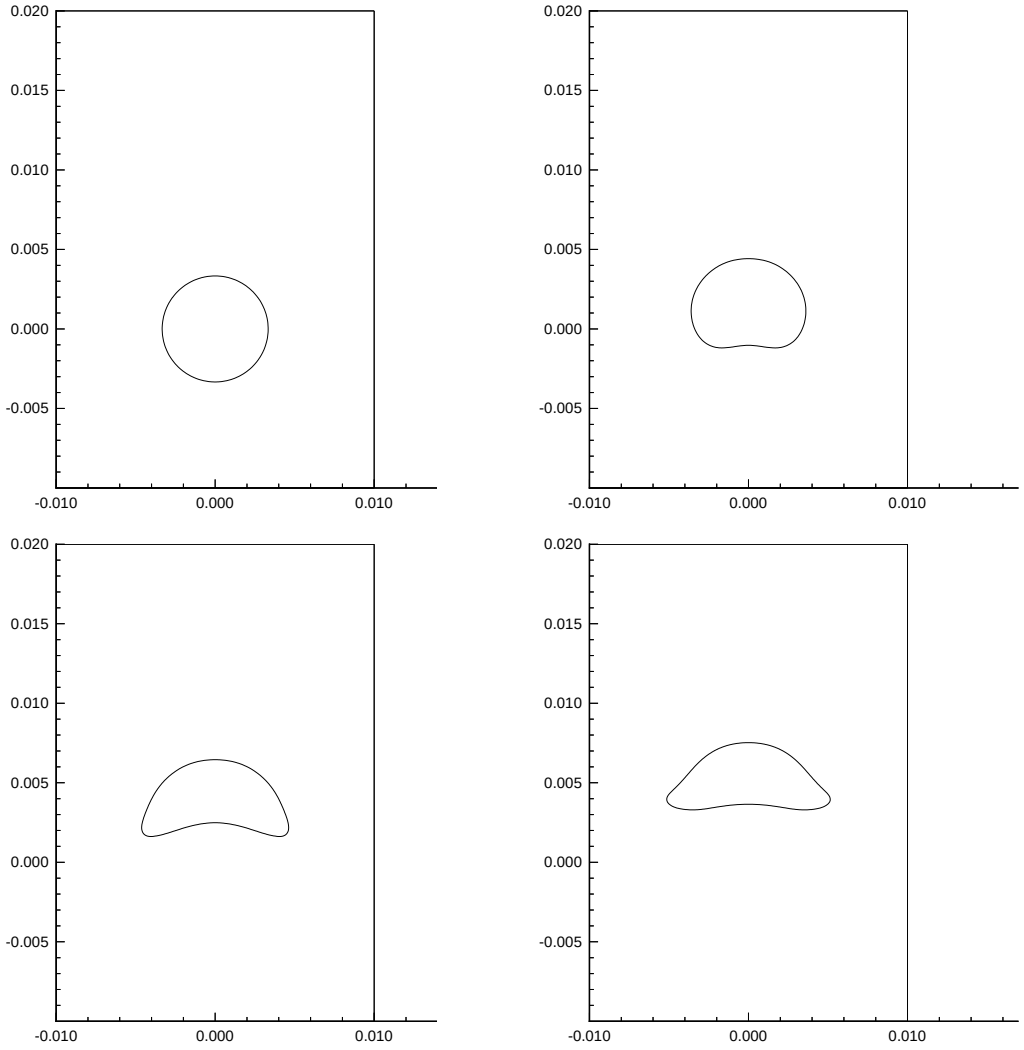

Figure 1: Rise of air bubble of radius 1/300m in water. A sequence of figures showing the interface development in time. Computations performed using a 300×300 grid.

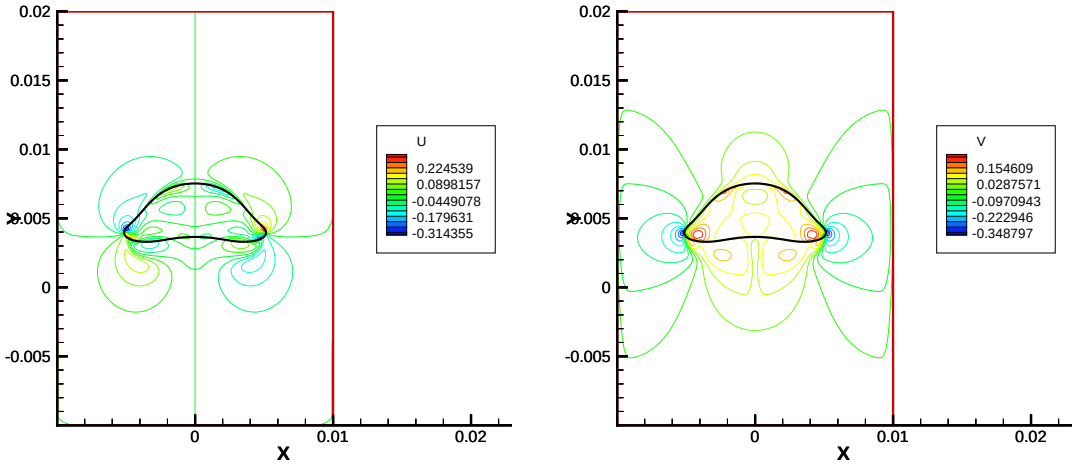

Figure 2: Contours of vertical velocity and location of air-water interface from results for rise of air bubble in water. Computations performed using a 300×300 grid.

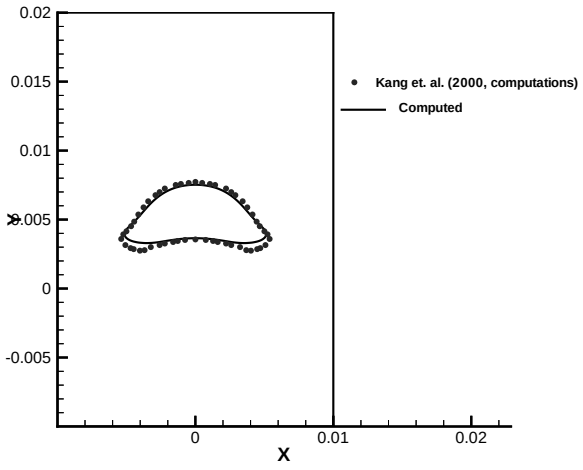

Figure 3: Comparison of air-water interface location at t=0.05s with computational results of Kang et. al. (2000). Computations performed using a 300×300 grid.

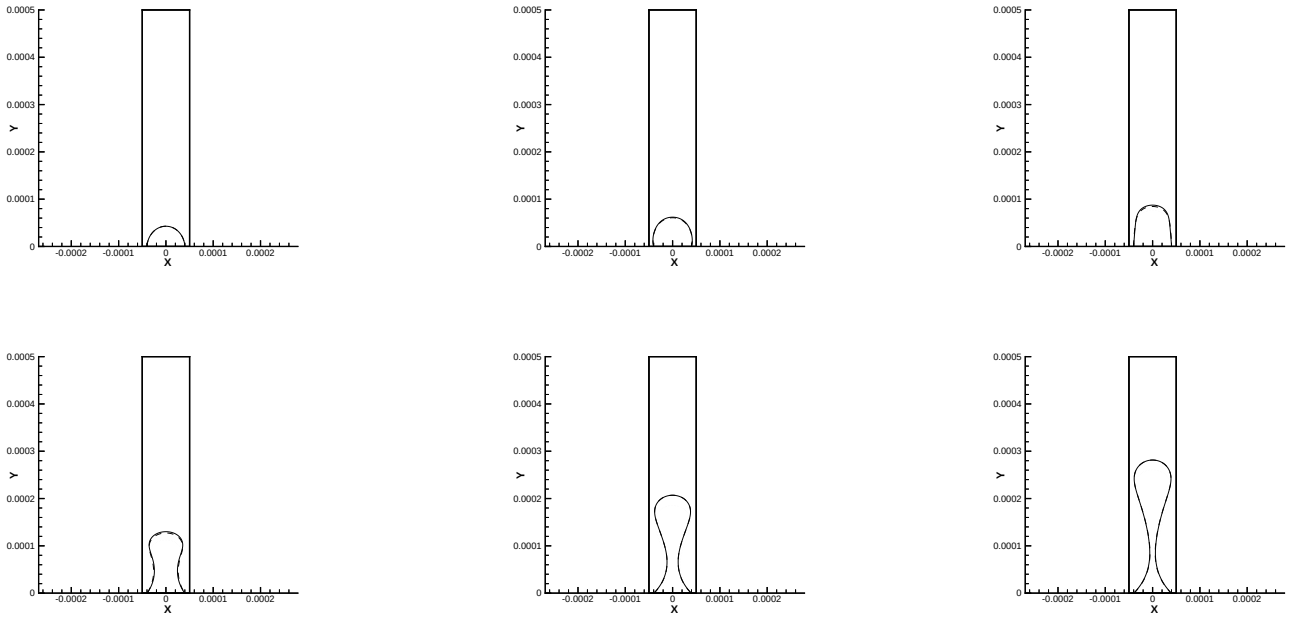

Figure 4: Sequence of figures, each showing pressure contours and phase boundaries, illustrating the formation of bubbles in 2-D microchannel. Computations for air and water as the two fluids and domain size of $100\mu m \times 500\mu m$. Simulations performed using 33×161 (dotted) , 65×321 (dashed lines), and 129×641 grids (solid lines) as a part of grid independence study.

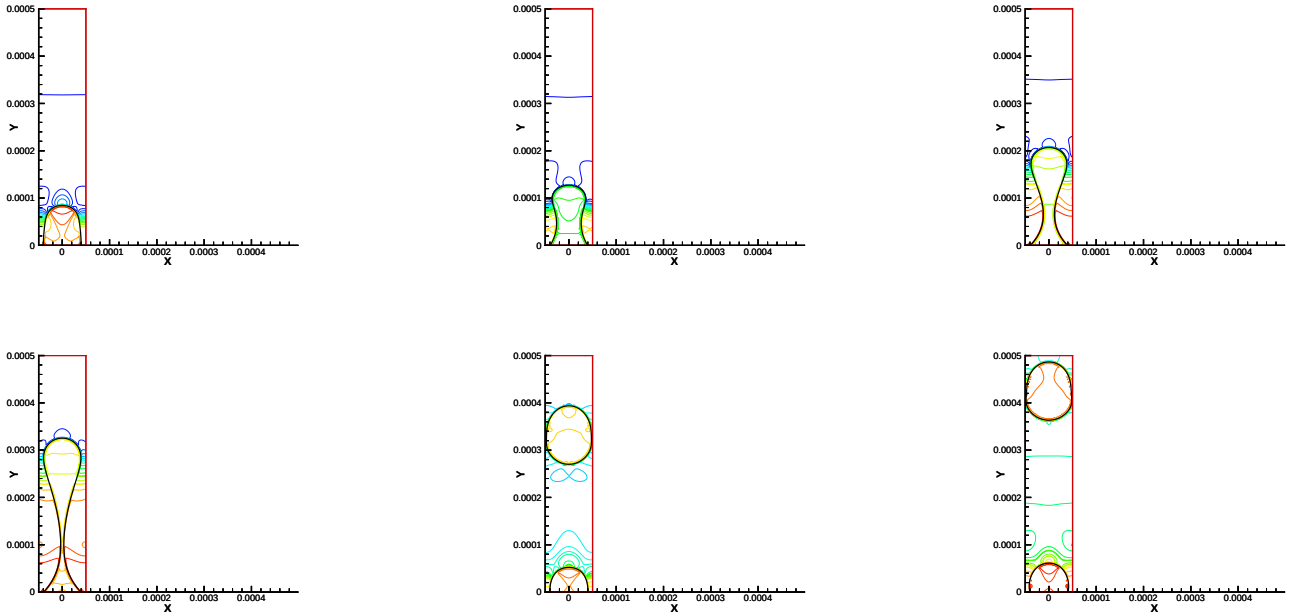

Figure 5: Sequence of figures, each showing pressure contours and phase boundaries, illustrating the formation of bubbles in 2-D microchannel. Air and water considered as the two fluids with surface tension coefficient set as $0.0728 kg/s^2$.

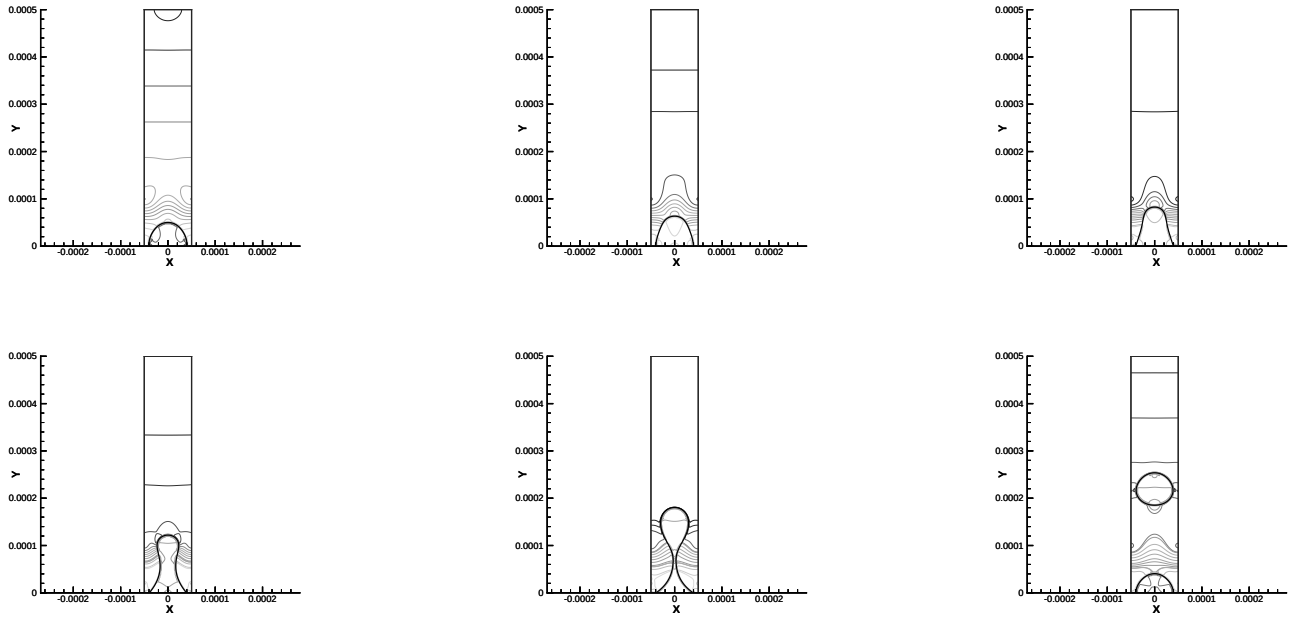

Figure 6: Sequence of figures, each showing pressure contours and phase boundaries, illustrating the formation of bubbles in 2-D microchannel. Test case with decreased surface tension of $0.01456 kg/s^2$.

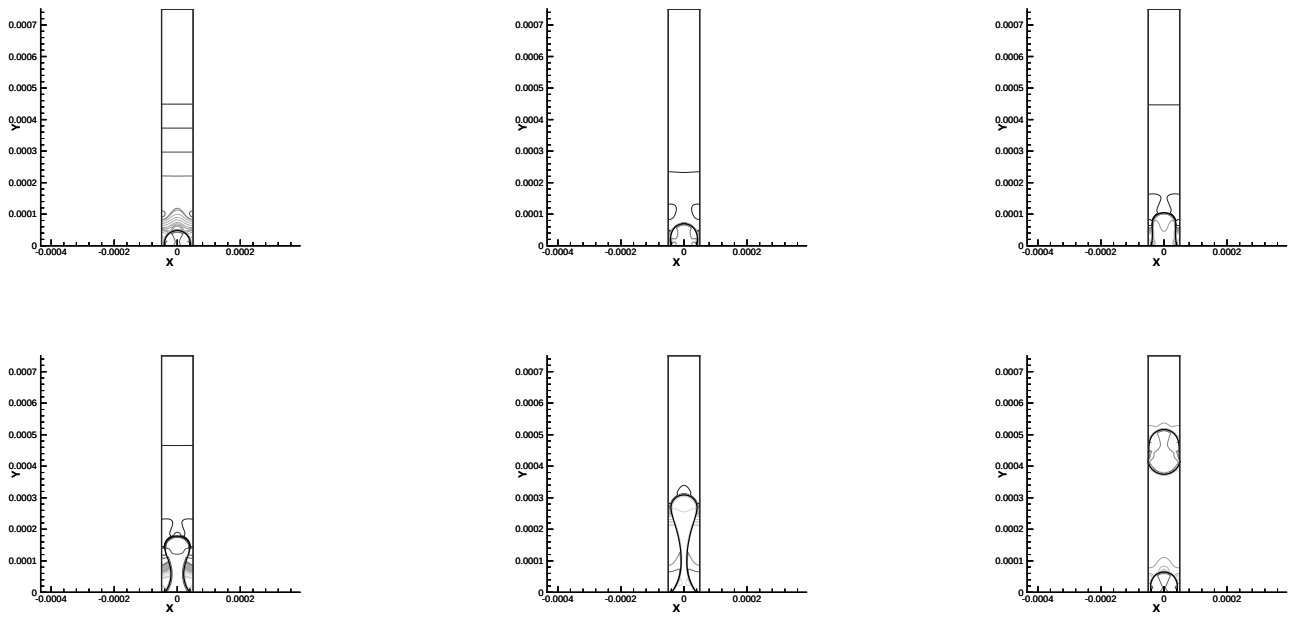

Figure 7: Sequence of figures, each showing pressure contours and phase boundaries, illustrating the formation of bubbles in 2-D microchannel. Test case with increased surface tension of $0.1456 kg/s^2$.

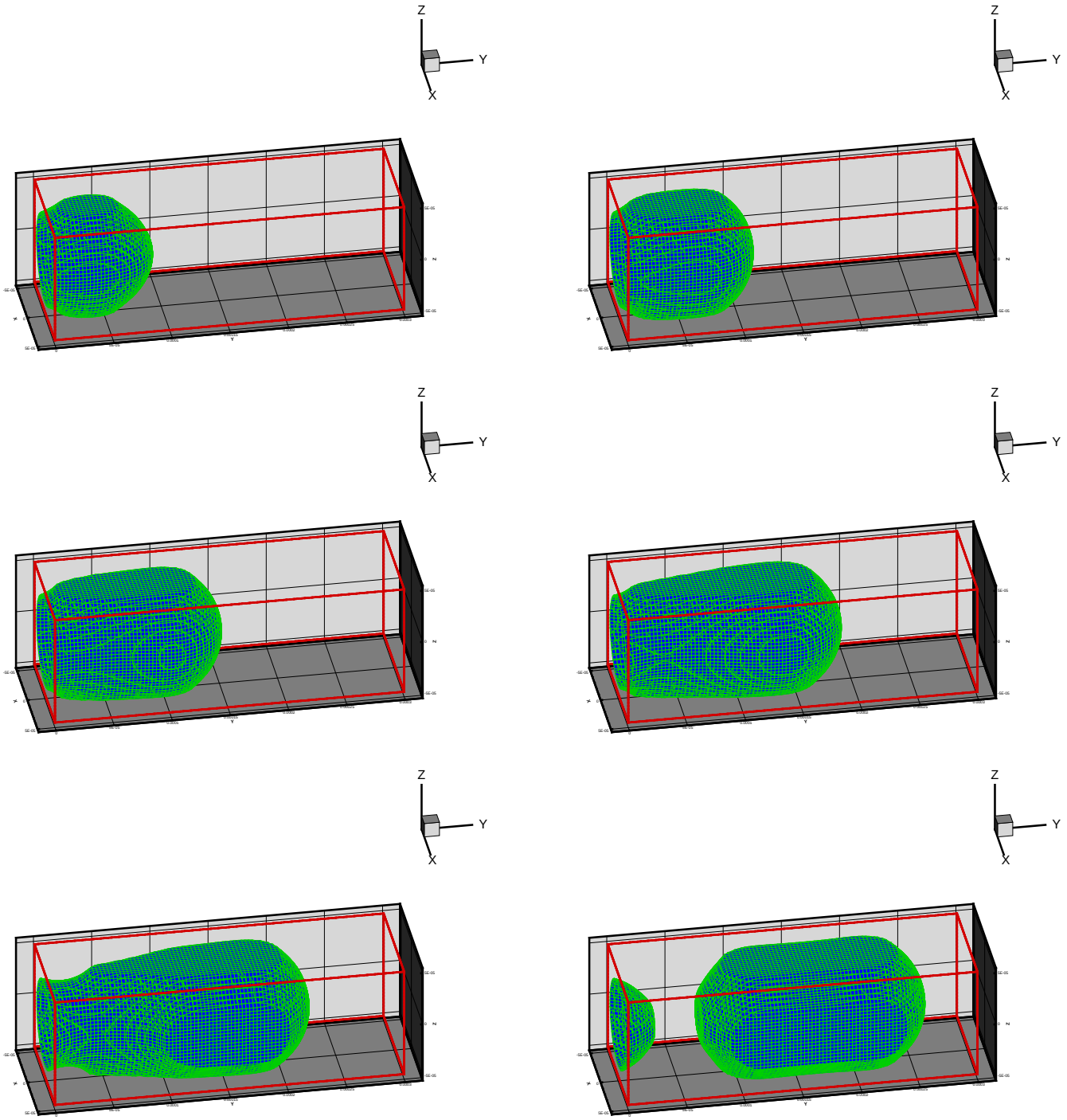

Figure 8: A sequence of figures showing the development and detachment of an air bubble in the crossflow mixing channel. Flow rates correspond to $Q_L/(Q_L + Q_G) = 0.5$.

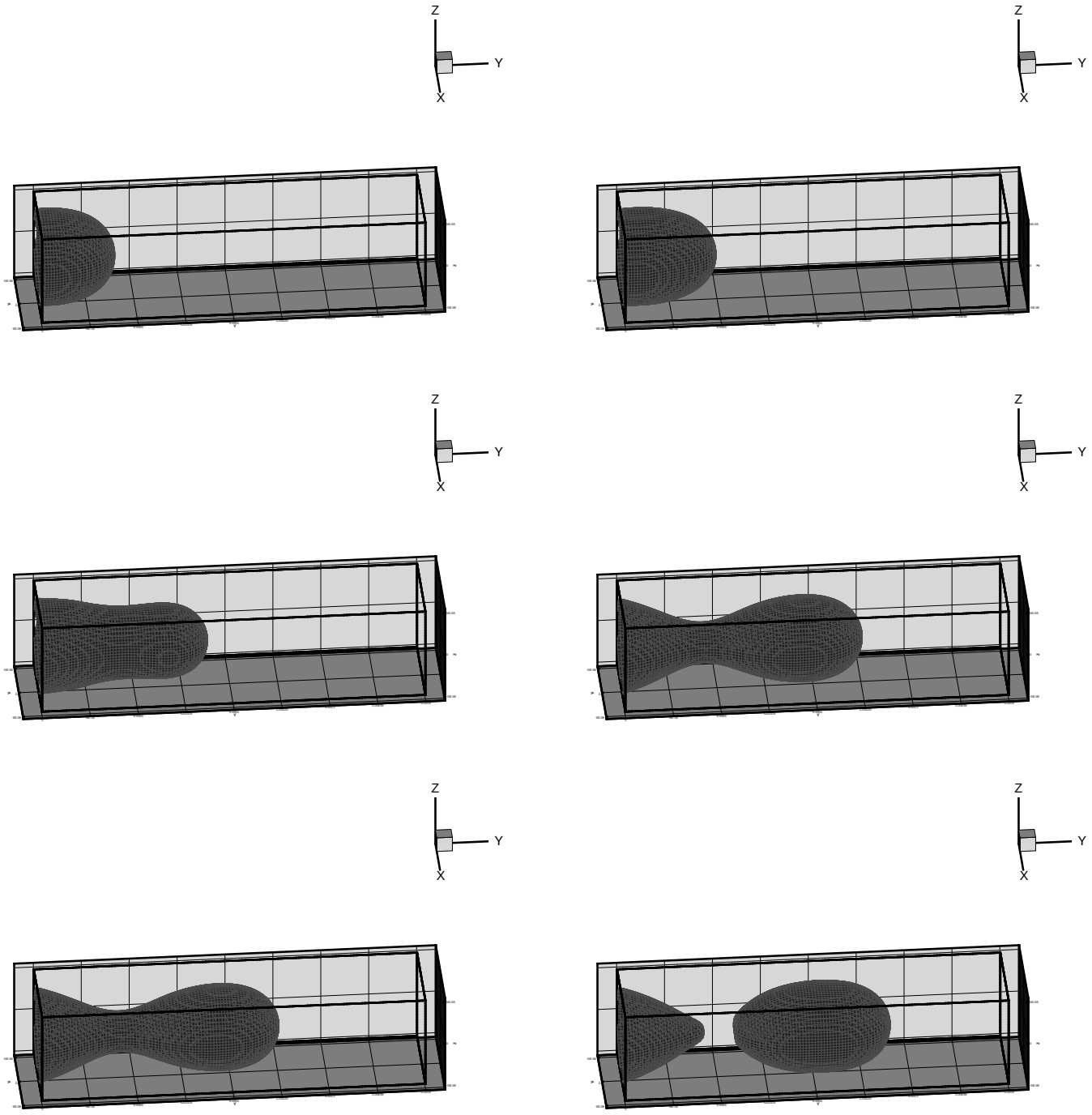

Figure 9: A sequence of figures showing the development and detachment of an air bubble in the crossflow mixing channel. Flow rates correspond to $Q_L/(Q_L + Q_G) = 0.67$.

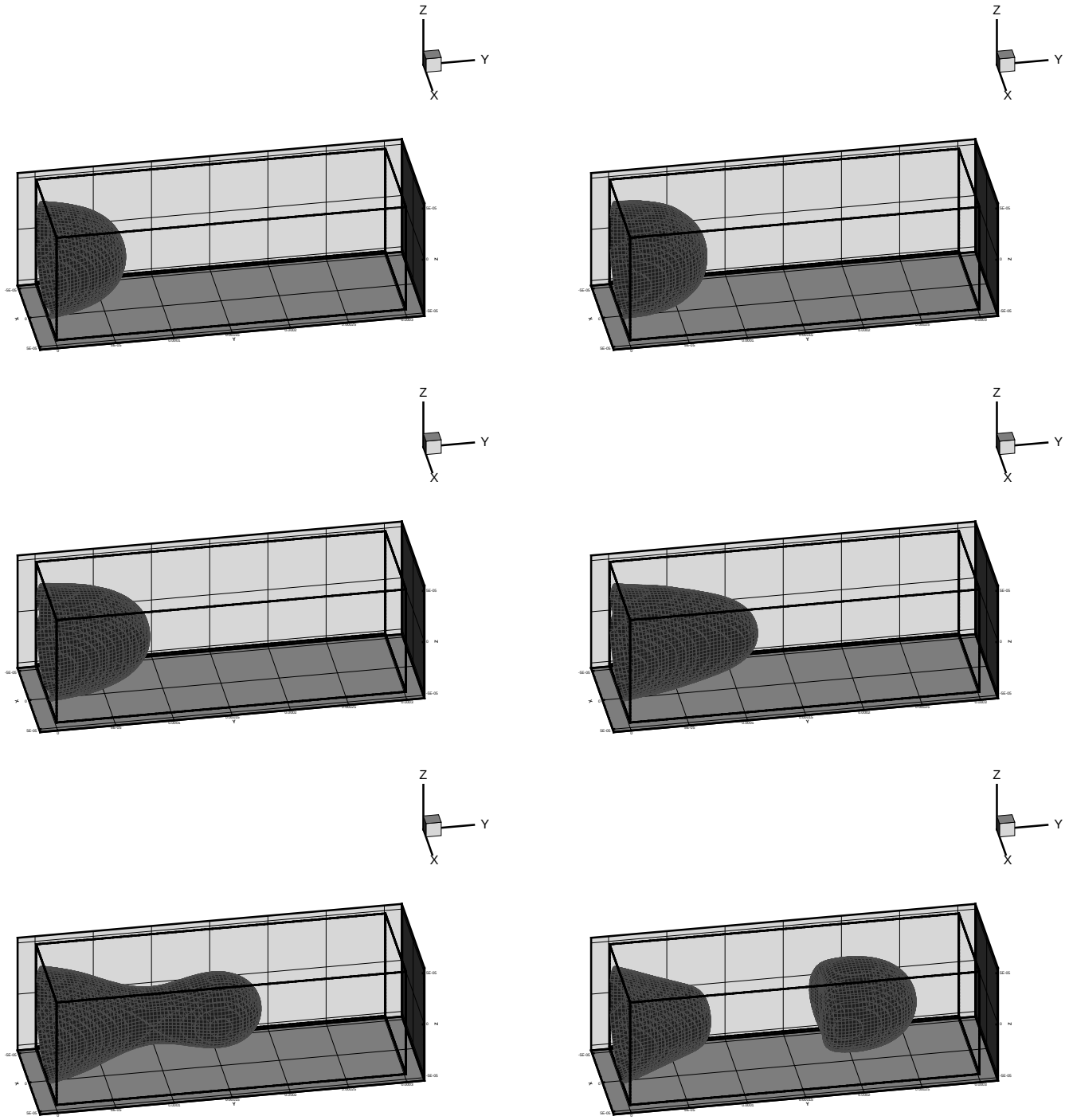

Figure 10: A sequence of figures showing the development and detachment of an air bubble in the crossflow mixing channel. Flow rates correspond to $Q_L/(Q_L + Q_G) = 0.8$.

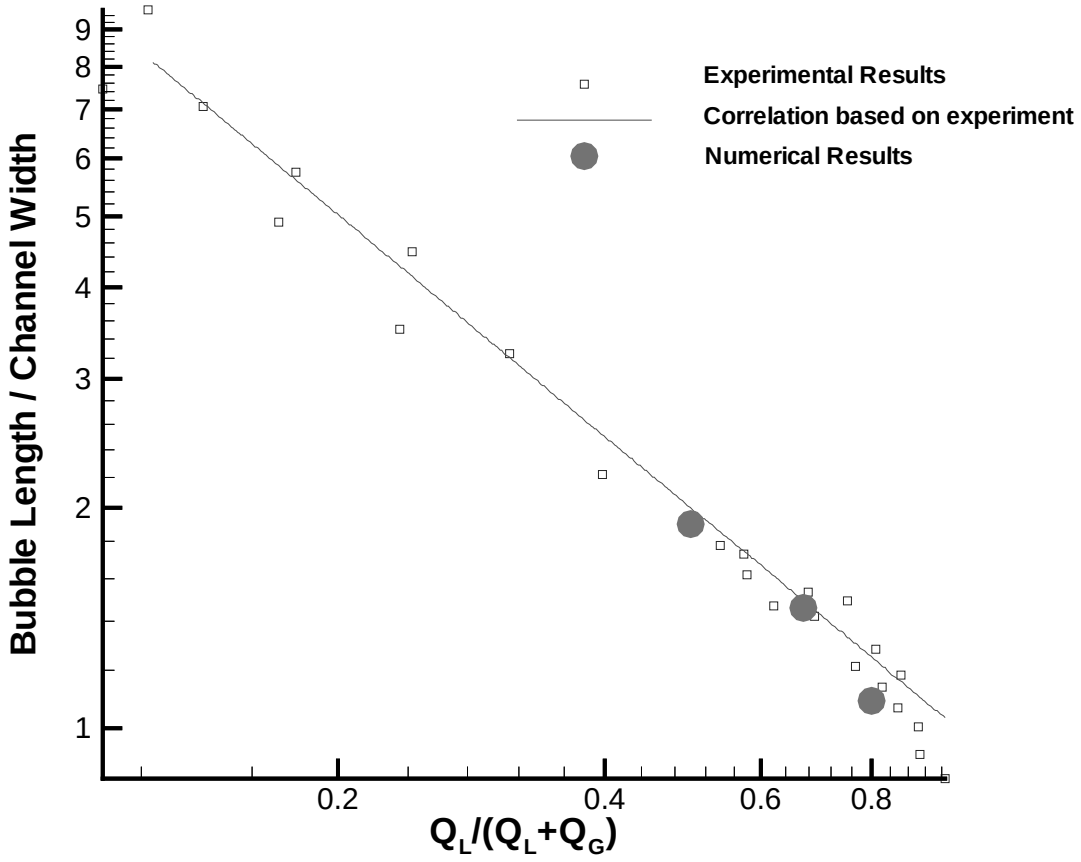

Figure 11: Comparison of numerically computed bubble sizes, for various flow rates, with experimental results of Cubaud et. al. [1].